IOCN 2022

MDPI

Proceeding Paper

Preparation and Characterization of Dithiocarbazate Loaded Mesoporous Silica Nanoparticles †

Thacilla Menezes [1,*], Tatiana Andreani [1,2] and Carlos Pereira [1]

[1] Chemistry Research Center (CIQ-UP), Faculty of Sciences of the University of Porto (FCUP), Rua do Campo Alegre 687, 4169-007 Porto, Portugal; tatiana.andreani@fc.up.pt (T.A.); cmpereir@fc.up.pt (C.P.)
[2] Research Centre of Sustainable Agrifood Production (GreenUPorto), Faculty of Sciences of the University of Porto (FCUP), Rua do Campo Alegre s/n, 4169-007 Porto, Portugal
* Correspondence: up201811986@edu.fc.up.pt; Tel.: +351-939-797-144
† Presented at the 3rd International Online-Conference on Nanomaterials , 25 April–10 May 2022; Available online: https://iocn2022.sciforum.net/

Abstract: Dithiocarbazates comprise an important class of Schiff bases that have remarkable pharmacological applications due to the imine group present in their structure. However, the lipophilic character of 1-(S-benzyldithiocarbazate)-3-methyl-5-phenyl-pyrazole (DTC) limits its gastrointestinal absorption leading to low oral bioavailability. Using DTC-loaded nanoparticles, such as mesoporous silica nanoparticles (MSiNP), synthesized by the Stöber method, which allows controlling pores, walls, and surfaces, can be an excellent strategy to overcome these drawbacks. In this sense, the present work reports the loading of DTC in MSiNP aiming at potential application in drug delivery and targeting.

Keywords: Schiff base; drug delivery systems; nanocarriers

Citation: Menezes, T.; Andreani, T.; Pereira, C. Preparation and Characterization of Dithiocarbazate Loaded Mesoporous Silica Nanoparticles. *Biol. Life Sci. Forum* **2022**, *2*, x. https://doi.org/10.3390/xxxxx

1. Introduction

Schiff bases are organic compounds that have been widely used since their first report by Hugo Schiff [1]. Thiosemicarbazones, semicarbazones, hydrazide/hydrazones and dithiocarbazates are compounds containing derived from the condensation of primary amines with aldehydes or ketones. Schiff bases are characterized by the presence of the bond > C=N, which is known to have significant biological and pharmacological properties [2], including antifungal, antibacterial, antiproliferative, anti-inflammatory, antiviral, antitumor, as well as for especially neglected diseases such as malaria, trypanosomiasis, and tuberculosis [3–6]. However, the lipophilic character of these compounds limits its administration resulting in low oral bioavailability. Such limitations can be overcome using drug delivery systems (DDS), which can provide more effective treatment regimens, control the dosage of drugs, and especially improve drug safety [7–9]. A compound extensively investigated in the scientific community as DDS are the mesoporous silica nanoparticles (MSiNP) created in 1960 as a catalyst, being later modified to improve their absorption properties, in 1968 by Stöber. MSiNP have several advantages due to their specific characteristics, such as: ordered pore network with homogeneous size (50 to 3000 nm); provide cavities that can host and release a wide variety of biomolecules and therapeutic agents; uniform and adjustable particle size and shape for each medical application; non-toxicity and biocompatibility [10,11]. In this sense, the focus of the present study was to synthesize and characterize a drug delivery system (DDS) for the delivery of dithiocarbazate (3-methyl-5-phenyl-pyrazoline-1-(S-benzyldithiocarbazate) (DTC)), based on a hybrid nanocarrier consisting of DTC adhered to the surface of mesoporous silica nanoparticles (MSiNP).

2. Materials and Methods

2.1. Synthesis of DTC

Dithiocarbazate compound, 1-(S-benzyldithiocarbazate)-3-methyl-5-phenyl-pyrazole, (DTC, $C_{18}H_{16}N_2S_2$) was synthesized according to previously reported procedures [12] by adding two drops of concentrated HCl in equimolar mixture of 4-phenyl-2,4-butanedione and the appropriate hydrazone in 10 mL of methanol (Scheme 1). The mixture was refluxed for 2 h and after DTC precipitation, the material was recrystallized from methanol and dried over anhydrous $CaCl_2$.

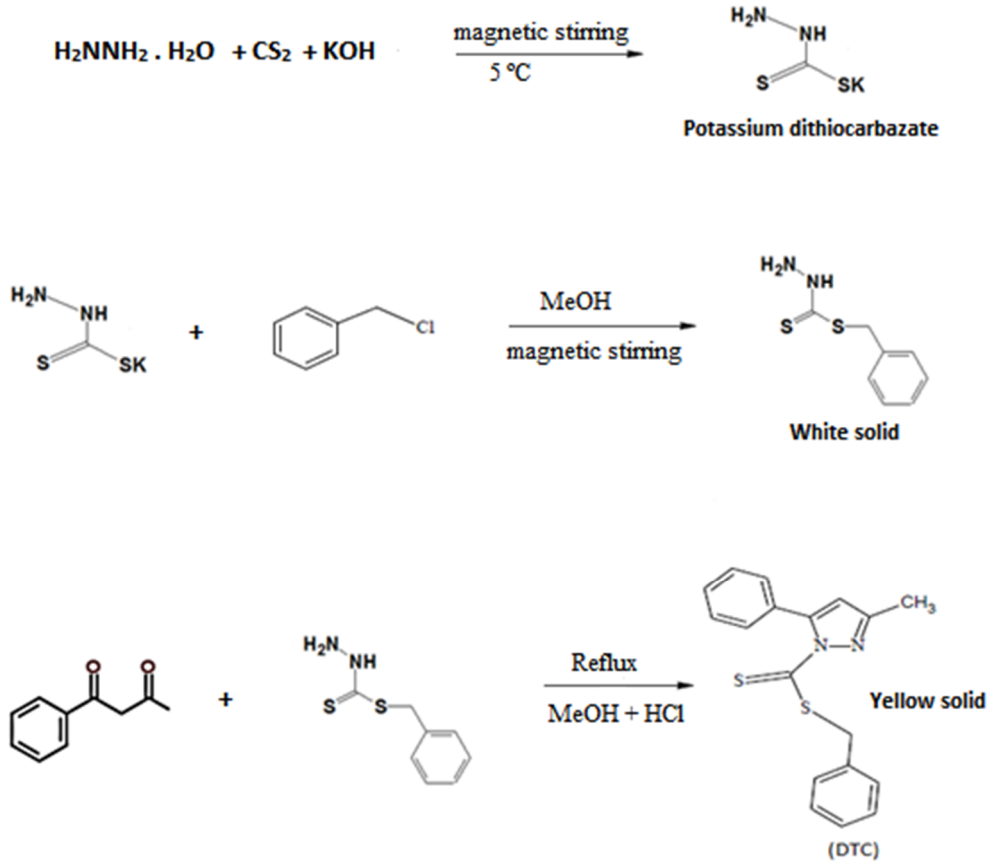

Scheme 1. Synthesis of 1-(S-benzyldithiocarbazate)-3-methyl-5-phenyl-pyrazole (DTC, $C_{18}H_{16}N_2S_2$).

2.2. Synthesis of MSiNP and MSiNP-DTC

Synthesis of MSiNP was carried out under a high concentration of precursors, which results in nanoparticles of highly uniform spherical shape (Scheme 2). For this procedure, 750 mg of cetyltrimethylammonium bromide (CTAB) was dissolved in 20 mL of an aqueous solution of NH_3 (0.048 mol L^{-1}) followed by homogenization under magnetic stirring in a round bottom distillation flask connected to a condenser reflux at 5 °C (to prevent evaporation of ethanol). To this solution, 3.2 mL of absolute ethanol was added as a co-solvent and the mixture was homogenized for 15 min at 60 °C. Sequentially, 2.5 mL of tetraethyl orthosilicate (TEOS) (1.2 mmol) was inserted in the solution and the flask kept at the same temperature for 2 h with agitation. At the end of the reaction, the compounds were isolated by centrifugation and washed with absolute ethanol before extraction of the soft mold (CTAB). Finally, the sample was washed twice with absolute ethanol and dried at 60 °C for 24 h. The residual CTAB was removed in an inert atmosphere (N_2) at 550 °C with a rate of 3 °C/min for 5 h [13]. For DTC-loaded MSiNP, 5 mg of DTC were solubilized in 10 mL of acetone at 37 °C followed by the addition of 100 mg of MSiNP. The reaction was maintained for 2 h and then centrifuged at 15,000 rpm,

rinsed with distilled water, separated by a second centrifugation, and dried at 60 °C overnight.

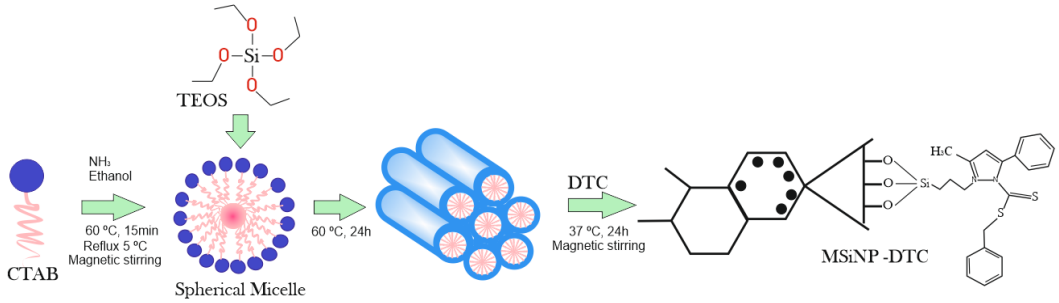

Scheme 2. Synthesis of MSiNP and MSiNP-DTC.

2.3. Suspensions and Characterization of MSiNP and MSiNP-DTC

Hydrodynamic diameter (Z-Ave) and PDI of the prepared MSiNP/MSiNP-DTC were determined by dynamic light scattering (DLS) using a Malvern Zetasizer Nano ZS90 (Malvern, United Kingdom) at 25 °C. The zeta potential (ZP) was determined by applying an electric field to the samples, and the values of the ZP were obtained by measuring the velocity of the electrophoretic mobility of the particles using the Doppler laser anemometry technique (Malvern Zetasizer Nano ZS (Malvern Instruments, Worcs, UK) at 25 °C. All samples were diluted in Milli-Q water (500 mg L^{-1}) by sonication for 30 min in an ultrasonic bath (Ultrasonic Cleaner, SONICA®, Soltec, Milan, Italy), and 1 mL was used for the analysis. Data were expressed as mean ± standard deviation (SD) of three measurements.

2.4. Transmission Electron Microscope (TEM) Analysis

The morphology of nanoparticles was checked by transmission electron microscopy (TEM) (Hitachi model H8100, with LaB6 filament and using an accelerating voltage of 200 kV). Images were acquired with an Olympus Keenview CCD camera (formerly Soft Imaging). MSiNP and MSiNP-DTC were dispersed in Milli-Q water by sonication for 30 min in an ultrasonic bath and placed on copper grids covered with carbon coating for TEM observations.

2.5. Fourier Transform Infrared (FT-IR)

FT-IR spectra were performed using a Bruker Vector 22 spectrometer in the 400–4000 cm^{-1} region. Loaded and unloaded silica nanoparticles were mixed with suitable amount of micronized KBr powder and compressed into disks with a force of 10 kN using a manual press to prepare the tablet. For each spectrum, an interferogram of 100 scans was collected with a resolution of 4 cm^{-1} in the medium infrared region at 25 °C.

2.6. Thermal Analysis

Differential scanning calorimetry (DSC) analyzes were performed using a DSC 7020 (Hitachi High-Tech Science Corporation, Japan). Analysis was performed with about 10 mg of MSiNP placed in an aluminum pan (7.5 µL), which was hermetically sealed. Scans were carried out from 25 to 600 °C at a heating rate of 5 °C min^{-1} under nitrogen atmosphere (100 mL min^{-1}). Data were obtained through the calculated area using Hitachi DSC 7020 software.

2.7. Entrapment Efficiency

Briefly, 5 mg of MSiNP-DTC were dispersed in 1 mL of ethanol and centrifuged at 13,500 rpm for 30 min. Then, 200 μL of supernatant was removed and diluted with ethanol to 500 μL and analyzed by UV-visible spectroscopy at 303 nm, using T70 UV-VIS Spectrometer PG Instruments Ltd. Data were expressed as mean ± SD of three measurements. The entrapment efficiency (% EE) (1) and the drug load (% DL) (2) were determined by the following Equations (1) and (2), respectively.

$$\%\boldsymbol{EE} = \frac{(\boldsymbol{Amount\ of\ initial\ DTC} - \boldsymbol{Amount\ of\ free\ DTC})}{\boldsymbol{Amount\ of\ initial\ DTC}} \times \mathbf{100} \quad (1)$$

$$\%DL = \frac{(\boldsymbol{Amount\ of\ initial\ DTC} - \boldsymbol{Amount\ of\ free\ DTC})}{\boldsymbol{Total\ Nanoparticle}} \times 100 \quad (2)$$

2.8. Nitrogen Adsorption

The surface areas of the different mesoporous silica grades were determined by nitrogen adsorption at −196 °C using a TriStar II Plus 2.02 from Micrometrics. Specific surface areas (SBET) were calculated by using the Brunauer–Emmett–Teller (BET) method. Pore size distribution and pore volume were estimated from the desorption branch of the N_2 adsorption–desorption isotherms by applying the Barrett–Joyner–Halenda (BJH) method. Measurements were performed in triplicate for each sample and the data were represented by mean ± SD.

3. Results and Discussion

MSiNP were synthesized using a positively charged CTAB as template and NH_3 as catalytic agent in aqueous conditions, through hydrolysis and condensation of tetraethoxsilane. After the reaction, the nanoparticles were loaded with Schiff's base (DTC) to be used as a drug release model. For this type of system, it is extremely important to evaluate the size and stability of the nanoparticles since these properties influence the in vivo performance. The results show a Z-Ave ranging from 168.4 ± 3.9 nm for unloaded MSiNP to 175.7 ± 1.0 nm for MSiNP-DTC, which corroborated that the encapsulation of DTC in MSiNP did not change the size of the nanoparticles. Concerning the PDI, the obtained values for both unloaded and loaded nanoparticles suggest monodispersing formulations, resulting in values of 0.29 ± 0.02 and 0.38 ± 0.04, for MSiNP and MSiNP-DTC respectively. ZP values for MSiNP changed from positive 16.8 ± 0.2 mV to negative values −11.7 ± 0.4 mV after calcination in a nitrogen atmosphere, due to neutralization of the ionizable fraction (residual silanol groups (Si-OH)) of the nanoparticles. After surface modification with DTC, higher ZP values (−21.9 ± 0.3 mV) were observed in comparison with unloaded nanoparticles.

TEM was used to evaluate the size, structure, and morphology of nanoparticles. Figure 1 shows the formation of spherical MSiNP with particle size around 48.0 ± 5.2 nm for MSiNP and 47.0 ± 6.0 nm for MSiNP-DTC. Furthermore, the TEM image clearly shows the mesoporous structure and that surface modification with DTC had no impact on the size, shape, and morphology of MSiNP. The reduction of the average diameter observed in TEM agrees with the Z-Ave obtained by DLS measurements, because the size of dried structure analyzed by TEM must be smaller than the same structure with the solvation layer around its surface analyzed by DLS [14].

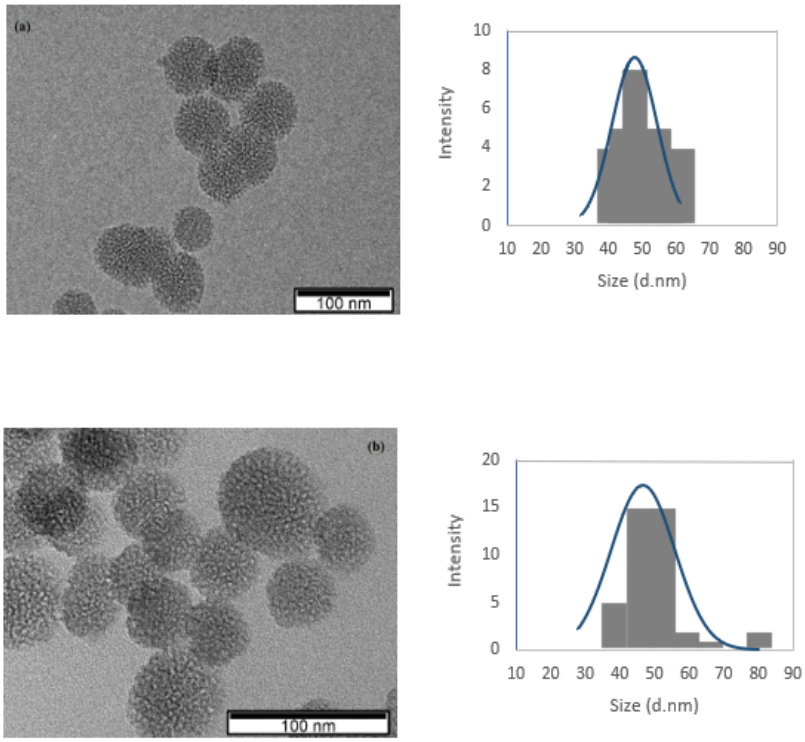

Figure 1. TEM images of (**a**) MSiNP and (**b**) MSiNP-DTC and their Histograms (size distributions) calculated by ImageJ (V 1.8.0).

The FT-IR spectra of DTC, MSiNP and MSiNP-DTC are shown in Figure 2 and Figure 3, respectively. DTC has two intense bands at 1574 and 1031 cm^{-1}, which can be assigned to the ν(C=N) and ν(N–N) modes, respectively (Figure 2). These bands are extremely important because they refer to the imine group, and a possible shift in their frequencies may be indicative of DTC encapsulation in silica matrix, in which a shift to lower frequencies is associated with a reduced binding order, while the shift to higher frequencies corresponds to an increase in the connection order. Figure 3 shows the spectra from MSiNP (a), MSiNP calcined (b) and MSiNP-DTC (c). The absorption band around 1096 cm^{-1} is due to the vibrations of asymmetric stretching of Si–O–Si, which indicates the presence of silica in the MSiNP, while the peaks at 807 and 468 cm^{-1} attributed to the groups Si–O–Si are symmetrical stretching and flexing vibrations, respectively (Figure 3a).

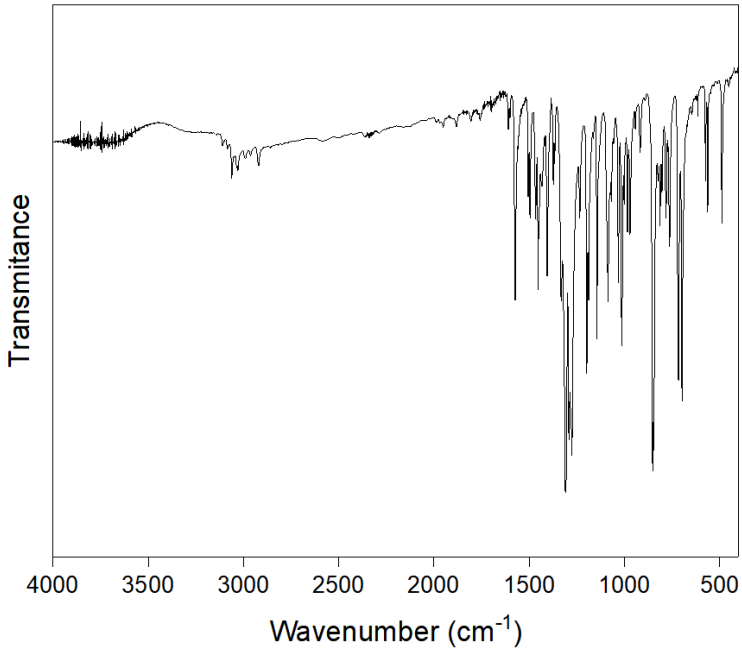

Figure 2. Vibrational spectrum in the infrared region of the compound DTC in KBr.

In the spectrum of MSiNP-DTC, it was not observed the appearance of new bands (Figure 3c). However the main bands of DTC that were reported above (Figure 2), suffered displacement increasing the intensity of the bands related to silica, (1627 cm^{-1}), and thus, we can infer that it is the vibration band ν(C=N); 1096 cm^{-1} shows the bands ν(N–N) and ν(N–N); 963 cm^{-1} ν(N–N); 796 cm^{-1} ν(SCS) and finally at 475 cm^{-1} the band ν(CSC) [15–18].

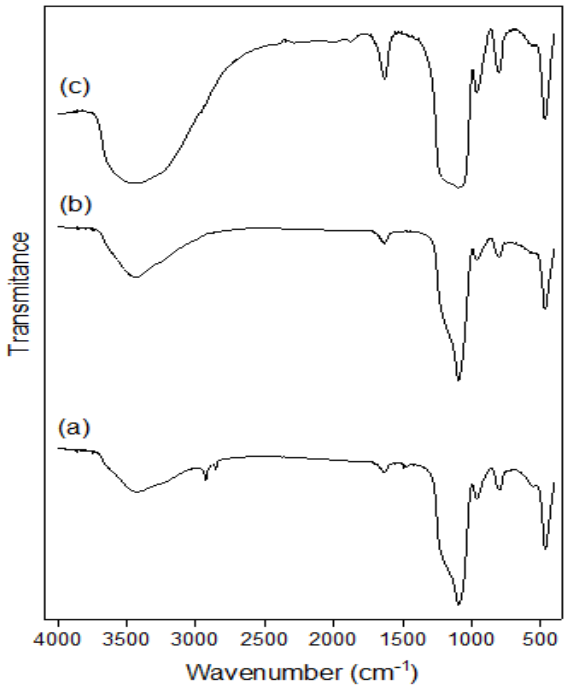

Figure 3. Vibrational Spectrum in the Infrared region of the MSiNP (**a**), MSiNP calcined (**b**) and MSiNP-DTC (**c**).

The thermal studies of all samples were carried out within a temperature range of 25–600 °C under the dynamic atmosphere of nitrogen to investigate their thermal stability.

For DTC, the thermal analysis was previously performed by Costa et al., (2019) [19] in which DSC presented an intense and sharp endothermic peak at 107 °C attributed to the melting process and at 300 °C associated with the process of decomposition or evaporation of the sample. Figure 4 illustrates the DSC profiles of MSiNP and DTC-loaded MSiNP. As MSiNP did not have any transitions in the temperature range of 25–600 °C (Figure 4a), only the thermal transition of MSiNP-DTC was observed. Thus, a melting endothermic peak at around 104 °C was observed in the thermogram of MSiNP-DTC (Figure 4b), which is indicative of a crystalline state of the drug, confirming DTC loading into MSiNP [20].

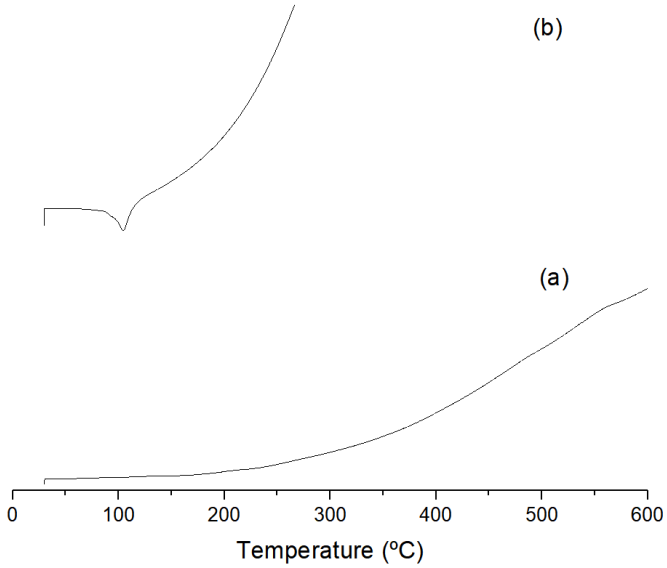

Figure 4. DSC profiles of MSiNP (**a**) and MSiNP-DTC (**b**).

It is known that inorganic carriers such as MSiNP tend to have high loading capacity but low loading efficiency, unlike organic carriers such as micelles, liposomes, and polymeric nanoparticles [21]. However, in this study, MSiNP-DTC maintained an efficient drug load (4.79 ± 0.04%) and high entrapment (95.77 ± 0.08%) capacity that may result from strong electrostatic and hydrogen bonding interactions between DTC and silica matrix. Furthermore, MSiNP exhibited a high BET surface area of 1021.05 ± 14.6 m^2/g, pore volume of 1.61± 0.04 cm^3/g, and mean pore size of 6.29 ± 0.1 nm. For MSiNP-DTC, the measured surface area and pore volume were estimated to be 617.99 ± 15.3 m^2/g and 1.01 ± 0.01 cm^3/g, respectively, while the mean pore size calculated from the N_2 adsorption–desorption isotherm was 6.52 ± 0.1 nm. In Figure 5, graphs (a) and (b) show the adsorption-desorption isotherms of MSiNP and MSiNP-DTC, respectively and correspond to type IV adsorption-desorption isotherms according to IUPAC, which are typical for materials with mesoporous structures with cylindrical pores [22]. On the other hand, the mean pore size for MSiNP-DTC does not decrease or even increase slightly, which may be an indication that pore entry is blocked (this is also confirmed by the large decrease in specific surface area and volume of the pore) due to the size of DTC molecule. Although such a change in textural properties occurred after binding DTC, the MSiNP containing DTC still maintained the typical mesoporous structure during the immobilization process [17,23].

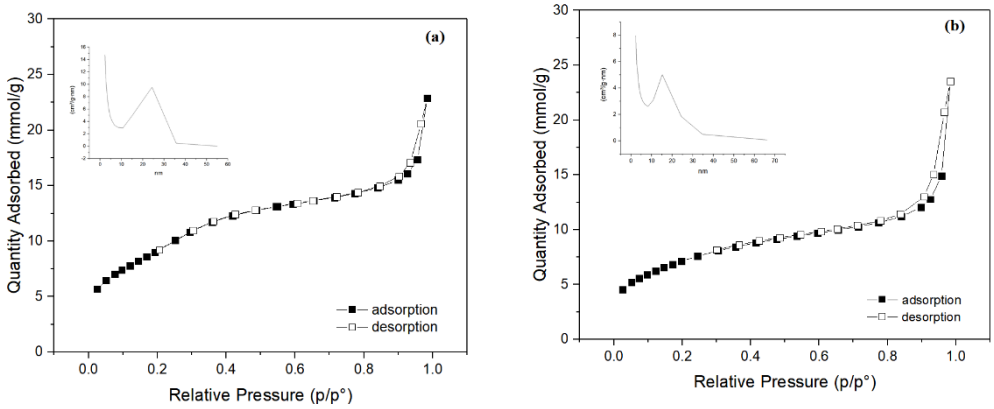

Figure 5. Nitrogen isotherms from MSiNP (**a**) and MSiNP-DTC (**b**).

4. Conclusions

In conclusion, DTC compound was successfully synthesized and loaded into the mesoporous matrix MSiNP by means of a simple and efficient synthesis. The characterization of the obtained MSiNP shows that nanoparticles have sizes suitable for drug delivery systems (DDS), stable in aqueous solutions which suggests monodisperse dispersions. Zeta potential analysis showed a shifted to negative values of MSiNP when loaded with DTC, which may indicate the successful adsorption at MSiNP surface. FTIR analysis showed that DTC loading did not induce changes in the bands in comparison with unloaded nanoparticles. However, the FTIR spectra suffered major bands DTC displacement, increasing the intensity of the bands related to silica matrix. Regarding to the nitrogen adsorption results, the pore size was larger after loading DTC in MSiNP and this may be related to the DTC being present on the matrix surface instead of the pores. Concerning to the loading efficiency of MSiNP, DTC was successfully incorporated in MSiNP, and these results suggest that MSiNP-DTC have potential for the use in drug delivery applications, improving stability and overcoming the low water solubility of Schiff's dithiocarbazate bases.

Author Contributions: Conceptualization, T.M. and T.A.; methodology, T.M. and C.P.; formal analysis, T.I.M, T.A. and C.P.; investigation, T.I.M, T.A. and C.P.; writing—original draft, T.I.M; writing—review and editing, T.I.M, T.A. and C.P.; supervision: T.A. and C.P.; resources, C.P.; funding acquisition, C.P. All authors have read and agreed to the published version of the manuscript.

Acknowledgments: T.I. Menezes thanks the NORTE2020 through project Norte-08-5369-FSE-000050 for financial support of a PhD grant. This work was partially supported by the FCT under Research Grant UIDB/00081/2020—CIQUP

Conflicts of Interest: The authors declare that they have no conflict of interest.

References

1. Jin, V.X.; Tan, S.I. Platinum (II) Triammine Antitumour Complexes: Structure-Activity Relationship with Guanosine 5′-MoJin, V.X.; Tan, S.I.; Ranford, J.D. Platinum (II) Triammine Antitumour Complexes: Structure-Activity Relationship with Guanosine 5′-Monophosphate (5′-GMP). *Inorg. Chim. Acta* **2005**, *358*, 677–686. https://doi.org/10.1016/j.ica.2004.09.024.
2. Zangrando, E.; Begum, M.S.; Sheikh, M.C.; Miyatake, R.; Hossain, M.M.; Alam, M.M.; Hasnat, M.A.; Halim, M.A.; Ahmed, S.; Rahman, M.N.; et al. Synthesis, Characterization, Density Functional Study and Antimicrobial Evaluation of a Series of Bischelated Complexes with a Dithiocarbazate Schiff Base Ligand. *Arab. J. Chem.* **2017**, *10*, 172–184. https://doi.org/10.1016/j.arabjc.2016.07.019.
3. Costa, A.R.; França, R.N.; Silva-Jardim, I.; Silva, R.J.S.; Lima-Santos, J.; Salay, L.C.; Santos, R.L.S.R. Self-Assembling Micellar System Based on Pluronic and Pyrazole-Dithiocarbazate-Conjugate Stimulates Production of Nitric Oxide from Macrophages. *Colloids Interface Sci. Commun.* **2021**, *41*, 100378. https://doi.org/10.1016/j.colcom.2021.100378.
4. de Menezes, T.I.; de Oliveira Costa, R.; Sanches, R.N.F.; de Oliveira Silva, D.; Santos, R.L.S.R. Preparation and Characterization of Dithiocarbazate Schiff Base–Loaded Poly(Lactic Acid) Nanoparticles and Analytical Validation for Drug Quantification. *Colloid Polym. Sci.* **2019**, *297*, 1465–1475. https://doi.org/10.1007/s00396-019-04572-9

5. Costa, A.R.; de Menezes, T.I.; Nascimento, R.R.; dos Anjos, P.N.M.; Viana, R.B.; de Araujo Fernandes, A.G.; Santos, R.L.S.R. Ruthenium(II) Dimethylsulfoxide Complex with Pyrazole/Dithiocarbazate Ligand: Synthesis, Spectroscopy Studies, DFT Calculations and Thermal Behavior. *J. Therm. Anal. Calorim.* **2019**, *138*, 1683–1696. https://doi.org/10.1007/s10973-019-08185-w.
6. Khan, M.F.; Alam, M.M.; Verma, G.; Akhtar, W.; Akhter, M.; Shaquiquzzaman, M. The Therapeutic Voyage of Pyrazole and Its Analogs: A Review. *Eur. J. Med. Chem.* **2016**, *120*, 170–201. https://doi.org/10.1016/j.ejmech.2016.04.077.
7. Freitas, L.B. de O.; Bravo, I.J.G.; Macedo, W.A. de A.; de Sousa, E.M.B. Mesoporous Silica Materials Functionalized with Folic Acid: Preparation, Characterization and Release Profile Study with Methotrexate. *J. Sol-Gel Sci. Technol.* **2016**, *77*, 186–204. https://doi.org/10.1007/s10971-015-3844-8.
8. Safari, J.; Zarnegar, Z. Advanced Drug Delivery Systems: Nanotechnology of Health Design A Review. *J. Saudi Chem. Soc.* **2014**, *18*, 85–99. https://doi.org/10.1016/j.jscs.2012.12.009.
9. Mamaeva, V.; Sahlgren, C.; Lindén, M. Mesoporous Silica Nanoparticles in Medicine-Recent Advances. *Adv. Drug Deliv. Rev.* **2013**, *65*, 689–702. https://doi.org/10.1016/j.addr.2012.07.018.
10. Stober, W., Fink, A., Bohn, E. Controlled growth of monodisperse silica spheres in the micron size range. *J. Colloid Interface Sci.* **1968**, *26*, 62–69. https://doi.org/ 10.1016/0021-9797(68)90272-5
11. Hassan, S.; Prakash, G.; Ozturk, A.; Saghazadeh, S.; Sohail, F.; Seo, J.; Dockmeci, M.; Zhang, Y.S.; Arabia, S. Evolution and clinical translation of drug delivery nanomaterials. *Nanotoday* **2018**, *15*, 91–106. https://doi.org/10.1016/j.nantod.2017.06.008.
12. Manan, M.A.F.A.; Tahir, M.I.M.; Crouse, K. a.; How, F.N.-F.; Watkin, D.J. Synthesis, Characterization and Antibacterial Activity of Schiff Base Derived from S-Methyldithiocarbazate and Methylisatin. *J. Chem. Crystallogr.* **2011**, *42*, 173–179. https://doi.org/10.1007/s10870-011-0220-6
13. Paula, A.J.; Martinez, D.S.T.; Júnior, R.T.A.; Filho, A.G.S.; Alves, O.L. Suppression of the Hemolytic Effect of Mesoporous Silica Nanoparticles after Protein Corona Interaction: Independence of the Surface Microchemical Environment. *J. Braz. Chem. Soc.* **2012**, *23*, 1807–1814. https://doi.org/10.1590/S0103-50532012005000048
14. Awad, E.; El-Fiqi, A.; Austin, D.; Lyndon, A. Possible Effect of Lesser Galangal (Alpinia Officinarum) Extracts Encapsulated into Mesoporous Silica Nanoparticles on the Immune Status of Rainbow Trout (Oncorhynchus N). *Aquac. Res*. **2020**, *51*, 3674–3684. https://doi.org/10.1111/are.14717.
15. Arriagada, F.; Günther, G.; Nos, J.; Nonell, S.; Olea-Azar, C.; Morales, J. Antioxidant Nanomaterial Based on Core–Shell Silica Nanospheres with Surface-Bound Caffeic Acid: A Promising Vehicle for Oxidation-Sensitive Drugs. *Nanomaterials* **2019**, *9*. https://doi.org/10.3390/nano9020214
16. Nhavene, E.P.F.; da Silva, W.M.; Trivelato Junior, R.R.; Gastelois, P.L.; Venâncio, T.; Nascimento, R.; Batista, R.J.C.; Machado, C.R.; Macedo, W.A. de A.; Sousa, E.M.B. de. Chitosan Grafted into Mesoporous Silica Nanoparticles as Benznidazol Carrier for Chagas Diseases Treatment. *Microporous Mesoporous Mater.* **2018**, *272*, 265–275. https://doi.org/10.1016/j.micromeso.2018.06.035.
17. Enache, D.F.; Vasile, E.; Simonescu, C.M.; Culita, D.; Vasile, E.; Oprea, O.; Pandele, A.M.; Razvan, A.; Dumitru, F.; Nechifor, G. Schiff Base-Functionalized Mesoporous Silicas (MCM-41, HMS) as Pb(Ii) Adsorbents. *RSC Adv*. **2018**, *8*, 176–189. https://doi.org/10.1039/c7ra12310h.
18. Nikoorazm, M.; Ghorbani-Choghamarani, A.; Noori, N. Oxo-Vanadium(IV) Schiff Base Complex Supported on Modified MCM-41: A Reusable and Efficient Catalyst for the Oxidation of Sulfides and Oxidative S-S Coupling of Thiols. *Appl. Organomet. Chem.* **2015**, *29*, 328–333. https://doi.org/10.1002/aoc.3295.
19. Costa, A.R.; de Menezes, T.I.; Nascimento, R.R.; dos Anjos, P.N.M.; Viana, R.B.; de Araujo Fernandes, A.G.; Santos, R.L.S.R. Ruthenium(II) Dimethylsulfoxide Complex with Pyrazole/Dithiocarbazate Ligand: Synthesis, Spectroscopy Studies, DFT Calculations and Thermal Behavior. *J. Therm. Anal. Calorim*. **2019**, *138*, 1683–1696. https://doi.org/10.1007/s10973-019-08185-w.
20. Ghaferi, M.; Zahra, S.W.; Shahmabadi, H.E.; Alavi, S.E. Enhancing the Efficacy of Albendazole for Liver Cancer Treatment Using Mesoporous Silica Nanoparticles: An in Vitro Study. *EXCLI J.* **2021**, *21*, 236–249. https://doi.org/10.21203/rs.3.rs-294729/v1
21. Hegazy, M.; Zhou, P.; Wu, G.; Wang, L.; Rahoui, N.; Taloub, N.; Huang, X.; Huang, Y. Construction of Polymer Coated Core-Shell Magnetic Mesoporous Silica Nanoparticles with Triple Responsive Drug Delivery. *Polym. Chem.* **2017**, *8*, 5852–5864. https://doi.org/10.1039/c7py01179b.
22. Talavera-Pech, W.A.; Esparza-Ruiz, A.; Quintana-Owen, P.; Vilchis-Nestor, A.R.; Carrera-Figueiras, C.; Ávila-Ortega, A. Effects of Different Amounts of APTES on Physicochemical and Structural Properties of Amino-Functionalized MCM-41-MSNs. *J. Sol-Gel Sci. Technol*. **2016**, *80*, 697–708. https://doi.org/10.1007/s10971-016-4163-4
23. Popova, M.D.; Szegedi, Á.; Kolev, I.N.; Mihály, J.; Tzankov, B.S.; Momekov, G.T.; Lambov, N.G.; Yoncheva, K.P. Carboxylic Modified Spherical Mesoporous Silicas Drug Delivery Carriers. *Int. J. Pharm.* **2012**, *436*, 778–785. https://doi.org/10.1016/j.ijpharm.2012.07.061